Leukodystrophy resembling Vanishing White Matter Disease is recapitulated by brain-specific depletion of apoptosis regulator MCL-1

Running title: MCL-1 is required for white matter integrity

Abigail H. Cleveland[1,2], Alejandra Romero[3], Laurent Alfonso Azcona[2], Melisa Herrero[4], Viktoriya D. Nikolova[5,6], Sheryl Moy[5,6], Orna Elroy-Stein[4,7], Vivian Gama[3,8,9] and Timothy R. Gershon[2,10,11]

[1]UNC Cancer Cell Biology Training Program, University of North Carolina, Chapel Hill, North Carolina 27599, USA

[2]Department of Neurology, UNC School of Medicine, University of North Carolina, Chapel Hill, North Carolina 27599, USA

[3]Vanderbilt University, Cell and Developmental Biology, Nashville, Tennessee 37232, USA .

[4]Shmunis School of Biomedicine and Cancer Research, Faculty of Life Sciences, Tel Aviv University, Tel Aviv, Israel

[5]UNC Carolina Institute for Developmental Disabilities

[6]Department of Psychiatry, UNC School of Medicine, University of North Carolina, Chapel Hill, North Carolina 27599, USA

[7]Sagol School of Neuroscience, Tel Aviv University, Tel Aviv, Israel

[8]Vanderbilt University, Vanderbilt Center for Stem Cell Biology, Nashville, Tennessee 37232, USA .

[9]Vanderbilt University, Vanderbilt Brain Institute, Nashville, Tennessee 37232, USA .

[10]UNC Neuroscience Center, University of North Carolina, Chapel Hill, North Carolina 27599, USA

[11]Lineberger Comprehensive Cancer Center, University of North Carolina, Chapel Hill, North Carolina 27599, USA

Co-corresponding authors: Vivian Gama (vivian.gama@vanderbilt.edu) and Timothy R. Gershon (gershont@neurology.med.unc.edu)

34
35
36

SUMMARY

Diverse mutations cause leukodystrophies through unresolved processes. Developing leukodystrophy therapies requires identifying mechanisms that operate downstream of causative mutations to produce white matter degeneration. We have identified the apoptosis regulator MCL-1 as required for white matter stability and depleted by leukodystrophy-causing mutations. Brain-specific deletion of *Mcl-1* in mice recapitulates progressive leukodystrophy, with MRI changes, decreased oligodendrocytes, and astrocytic and microglial changes typical of Vanishing White Matter Disease (VWMD). Disabling apoptosis through co-deletion of *Bax* or *Bak* rescued white matter *Mcl-1*-dependence, broadly implicating the intrinsic apoptotic pathway in leukodystrophy pathogenesis. *Bax* and *Bak* co-deletions rescued different aspects of the *Mcl-1*-deleted phenotype, demonstrating their discrete roles in white matter stability. MCL-1 protein abundance was reduced in *eif2b5*-mutant mice that model VWMD, suggesting a mechanistic relationship between MCL-1 and VWMD. Our data show that oligodendrocytes require MCL-1 to suppress apoptosis, implicate MCL-1 loss in VWMD pathogenesis, and suggest inhibiting apoptosis for leukodystrophy therapy.

Introduction

Leukodystrophies are a heterogeneous group of severe neurodegenerative disorders marked by progressive white matter disruption (Raymond, 2017, van der Knaap and Bugiani, 2017). The age of onset varies in each leukodystrophy, but patients typically become symptomatic during childhood, after a latent, asymptomatic period (Kohler et al., 2018, Kohlschutter and Eichler, 2011). Patients with leukodystrophies may experience progressive symptoms including ataxia,

dementia, hallucinations, seizures, coma, and death (Vanderver et al., 1993). There is currently no specific targeted therapy that has been clinically implemented to arrest the progression of any leukodystrophy.

Diverse pathogenic mutations have been linked to different leukodystrophies (van der Knaap and Bugiani, 2018), but the mechanistic processes through which specific mutations cause white matter degeneration are incompletely understood. Mutations in the apoptotic regulator *APOPT1* (aka *COA8*) cause Progressive Cavitating Leukoencephalopathy, suggesting a role for inappropriate apoptosis in this disease (Melchionda et al., 2014, Yasuda et al., 2006). However, it is not clear why this mutation specifically affects cells of the white matter. Mutations in *eIF2B* subunits result in Vanishing White Matter Disease (VWMD), another leukodystrophy similarly marked by white matter cavitation (Bugiani et al., 2018, van der Knaap et al., 1997, van der Knaap et al., 1993). The causative role of *eIF2B* mutations implicates impaired mRNA translational regulation in VWMD pathogenesis, associated with activation of the Integrated Stress Response (ISR) (van der Knaap et al., 2006, Fogli et al., 2002, Leegwater et al., 2001, Bugiani et al., 2010, Abbink et al., 2019, Kantor et al., 2005). Prior studies have not identified a role for apoptosis in VWMD causation, as seen in Progressive Cavitating Leukoencephalopathy, and whether a common pathogenic process unites these similar phenotypes is unclear.

Studies in *eIf2b5* $^{R132H/R132H}$ mice provide insight into the disproportionate effect of *eIF2B* mutations on white matter. These mice develop leukodystrophy resembling VWMD and show impaired mitochondrial function in fibroblasts, astrocytes, and oligodendrocytes (Herrero et al., 2019, Raini et al., 2017, Geva et al., 2010). These studies suggest that *eIF2B* mutations disproportionately affect white matter because glia are more dependent than other types cells on accurate

translational regulation and mitochondrial function (Elroy-Stein, 2017). However, several unresolved steps are required to connect the biological processes that have been found to be disrupted in Progressive Cavitating Leukoencephalopathy and VWMD to the observed disease process of progressive leukodystrophy.

Identifying proteins that are both required for white matter integrity and affected by *eIF2B* mutations may show specific mechanisms that link VWMD genotype and phenotype. Defining these mechanistic links may show why diverse leukodystrophy mutations produce the final common pathology of white matter degeneration. Identifying proximal mediators of white matter degeneration may also provide important insight into leukodystrophy pathogenesis and treatment.

Here we report that mice with conditional deletion of the anti-apoptotic regulator *Mcl-1* targeted to brain stem cells develop progressive postnatal white matter degeneration that recapitulates the phenotype of human leukodystrophies, particularly VWMD. MCL-1 promotes the survival of different cell lineages through its ability to inhibit the pro-apoptotic proteins BAK and BAX, the main effectors of cell death in mammalian cells. Importantly, MCL-1 is a mitochondrial protein that is translationally suppressed by ISR activity (Fritsch et al., 2007), while VWMD disrupts mitochondria and activates the ISR, raising the possibility the MCL-1 deficiency could play a role in the VWMD phenotype.

Mcl-1-deleted mice were born with normal brain anatomy and show normal motor control and behavior at postnatal day 7 (P7), but then develop increasingly severe ataxia, abnormal motor responses, and extensive white matter atrophy. This white matter-predominant neurodegenerative process closely matches the course of human leukodystrophies with similar postnatal onset of symptoms, MRI changes, progressive white matter degeneration, reduced oligodendrocyte populations,

astrocytic abnormalities, and microglial accumulation. Mutations that block the intrinsic apoptotic pathway rescued the phenotype of *Mcl-1* deletion, implicating apoptosis in leukodystrophy pathogenesis, and suggesting a potential approach to therapy.

Results

Conditional *Mcl-1* deletion in the CNS causes progressive white matter degeneration.

We generated mice with conditional, brain-specific *Mcl-1* deletion by breeding *Mcl-1*$^{loxP/loxP}$ mice that harbor loxP sites around exon 1 of the *Mcl1* locus (Dzhagalov et al., 2007), with *GFAP-Cre* mice that express Cre recombinase in stem cells that give rise to the neurons and glia of the cerebrum and cerebellum, excluding the Purkinje cells (Supp fig. 1A-B) (Zhuo et al., 2001, Kuang et al., 2012). The resulting *hGFAP-Cre/Mcl-1*$^{loxP/loxP}$ (*Mcl-1*^{cKO}) mice were born at the expected Mendelian ratio. We compared *Mcl-1*^{cKO} mice to littermate controls, including *Mcl-1*$^{loxP/loxP}$ mice without Cre and heterozygously deleted *hGFAP-Cre/Mcl-1*$^{loxP/+}$. We found no differences between control genotypes and therefore pooled them for analysis. In contrast, *Mcl-1*^{cKO} mice appeared normal at P7 but developed increasing ataxia, could not be weaned, and died between P20-23.

Examination of the brains of *Mcl-1*^{cKO} showed progressive white matter degeneration, that began after the first week of life, with relative sparing of gray matter. At P7, *Mcl-1*^{cKO} brains showed no abnormalities and appeared similar to

controls (Fig. 1A, P7). At P14, *Mcl-1*^{cKO} mice showed white matter rarefaction and ventricular dilation and these changes were more pronounced at P21 (Fig. 1, P14&21). In addition to white matter loss, we also noted migration abnormalities in the cerebellum, with ectopic cerebellar granule cells in the molecular layer of the cerebellum (Fig. 1). Replacing *Gfap-Cre* with *Nestin-Cre* which similarly drives recombination in multipotent glio-neuronal stem cells, generating mice with the genotype *Nestin-Cre/Mcl-1*$^{loxP/loxP}$, similarly resulted in white matter-specific degeneration (Supp Fig. 2). Deletion of *Mcl-1* throughout the brain thus resulted in progressive white matter pathology that began in the early postnatal period and increased over time.

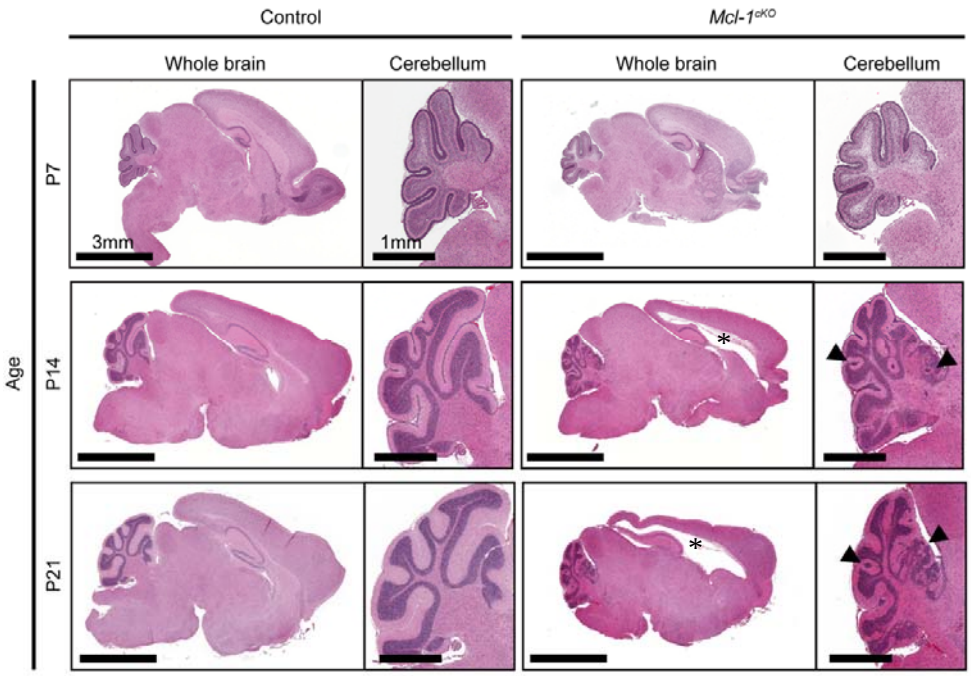

Figure 1. *Mcl-1* deletion causes progressive white matter degeneration. Brains of representative *Mcl-1*^{cKO} mice shown in H&E-stained sagittal sections appear similar to controls at P7. By P14, *Mcl-1*^{cKO} mice develop white matter degeneration with ventricular enlargement (*) and abnormal migration of cerebellar granule neurons (arrows). White matter loss increases by P21.

Consistent with the onset of neuropathology after P7, *Mcl-1*^{cKO} mice showed no behavioral deficits during the first week of life and gained weight similarly to controls but by P14, *Mcl-1*^{cKO} mice showed reduced weight gain (Fig. 2A) and progressive neurologic impairment. *Mcl-1*^{cKO} mice demonstrated progressive abnormalities of motor function. We used developmentally adjusted tests to compare behavior of *Mcl-1*^{cKO} mice and controls at P7, P14, and P18. To examine behavior at P7, when mice do not yet have open eyes and do not venture from the nest, we used a test of geotaxis by placing mice on a tilted screen and measuring latency to turn. We also measured latency to turn over in a righting test, and we counted pivots during a 3-min open field test. We found no genotype-specific differences at P7 (Table 1).

Test	WT	*Mcl-1*^{cKO}
Negative geotaxis (latency, s)		
Trial 1	15.4 ± 2	14.3 ± 3
Trial 2	15.1 ± 2	16.7 ± 3
Trial 3	15.3 ± 2	20.9 ± 3
Righting (latency, s)	8.2 ± 1	10.0 ± 3
Number of pivots	1.7 ± 0.3	1.3 ± 0.5

Table 1. Neonatal behavior testing showed no effects of *Mcl-1*^{cKO} genotype at P7. Each test was performed on 48 replicate WT pups and 13 replicate *Mcl-1*^{cKO} pups at P7. Measures included latency to turn on a tilted screen in a test for geotaxis, and latency to turn over in a righting test. Pivots were counted by an experimenter during a 3-min open field test. One-way ANOVA found no statistically significant differences.

In contrast to the similar behaviors at P7, by P14 *Mcl-1*^{cKO} mice showed decreased rearing when placed in an open field and spent more time in the center

of the open field, while traveling similar distances compared to controls (Fig. 2B; Supp fig. 1C). P18 *Mcl-1*^{cKO} mice also showed a marked increase in limb clasping when vertically suspended (Fig. 2C), a commonly used marker of disease progression in a number of mouse models of neurodegeneration and ataxia (Guyenet et al., 2010, Nakamura et al., 2016). Responses to sensory input were also abnormal in *Mcl-1*^{cKO} mice and changed over time. At P14, mice showed increased amplitude of acoustic startle response (Fig. 2D). By P21, when motor function was significantly impaired, the amplitude of acoustic startle response was markedly diminished compared to controls. *Mcl-1*^{cKO} mice thus show reduced inhibition in response to sensory stimuli at P14, and reduced motor responses at later ages. The motor and sensory tests show progressive behavior abnormalities that correspond temporally with the white matter degeneration, beginning at P12 and worsening by P18-21.

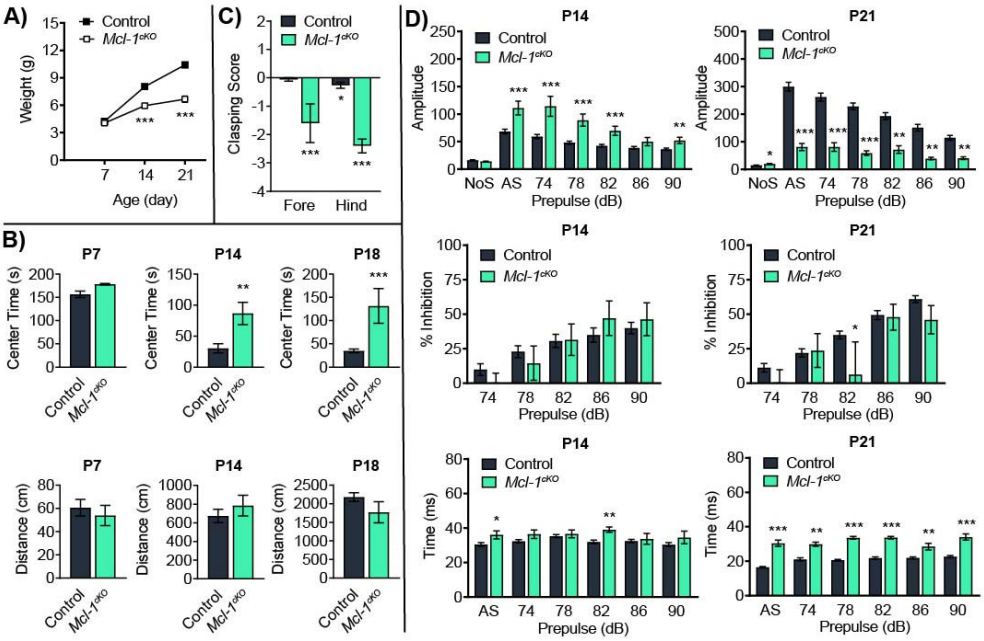

Figure 2. *Mcl-1* deletion causes progressive motor impairment and white matter degeneration. (**A**) Reduced weight gain in *Mcl-1*^{cKO} mice compared to controls. (**B**) *Mcl-1*^{cKO} mice show normal motor function at P7, with altered motor

function by P14 and (**C**) increased hind-limb clasping at P18. (**D**) *Mcl-1*^{cKO} mice show increased startle in response to auditory stimuli at P14, and reduced elicited movement at P21. *, ** and *** denote $p<0.05$, $p<0.01$ and $p<0.001$ respectively, relative to controls.

Blocking apoptosis prevents white matter degeneration in *Mcl-1*-deleted mice.

To determine if white matter degeneration in *Mcl-1*^{cKO} mice resulted from increased apoptosis, we examined cell death through cleaved caspase-3 immunohistochemistry and TUNEL assays. We did not detect an increase in cleaved caspase-3-stained cells at P7, prior to the onset of white matter loss, or at P14, after white matter loss was evident (data not shown). However, TUNEL staining, performed at P11 when white matter loss was developing, demonstrated increased cell death in *Mcl-1*^{cKO} brains, consistent with a pro-apoptotic effect of *Mcl-1* deletion (Fig. 3A).

To determine whether the increased cell death in *Mcl-1*-deleted mice was causally related to the white matter degeneration, we tested whether blocking apoptosis through co-deletion of either *Bax* or *Bak* rescued the *Mcl-1*^{cKO} phenotype. We repeatedly intercrossed *Mcl-1*^{cKO} mice with *Bax*$^{loxP/LoxP}$/*Bak*$^{-/-}$ mice to generate animals with conditional deletion of *Mcl-1* and heterozygous or homozygous deletion of *Bax* or *Bak*. We then raised pups of each genotype and analyzed survival, neurologic function, and neuropathology.

We found that co-deletion of *Bax* or *Bak* significantly suppressed the *Mcl-1*^{cKO} phenotype, but resulted in different, mitigated phenotypes. *Mcl-1*-deleted mice with heterozygous co-deletion of *Bak*, with the genotype *hGFAP-Cre/Mcl1*$^{loxP/loxP}$/*Bak*$^{-/+}$ (*Mcl-1*^{cKO}/*Bak*$^{-/+}$), showed normal survival without overt neurologic deficits and normal white matter and cerebellar migration (Fig. 3B). In

contrast, *Mcl-1*-deleted mice with heterozygous co-deletion of *Bax*, with the genotype *hGFAP-Cre/Mcl1*$^{loxP/loxP}$/*Bax*$^{loxP/+}$ (*Mcl-1*^{cKO}/*Bax*$^{fl/+}$), showed a progressive leukoencephalopathy phenotype similar *Mcl-1*^{cKO} mice (Fig. 3B). Immunohistochemistry demonstrated markedly lower BAK protein in *Bak*$^{+/-}$ animals (Fig. 3C), indicating that that heterozygous *Bak* deletion was sufficient to alter BAK expression. The rescued phenotype of *Mcl-1*^{cKO}/*Bak*$^{-/+}$ mice therefore demonstrated reducing BAK protein expression was sufficient to prevent white matter degeneration.

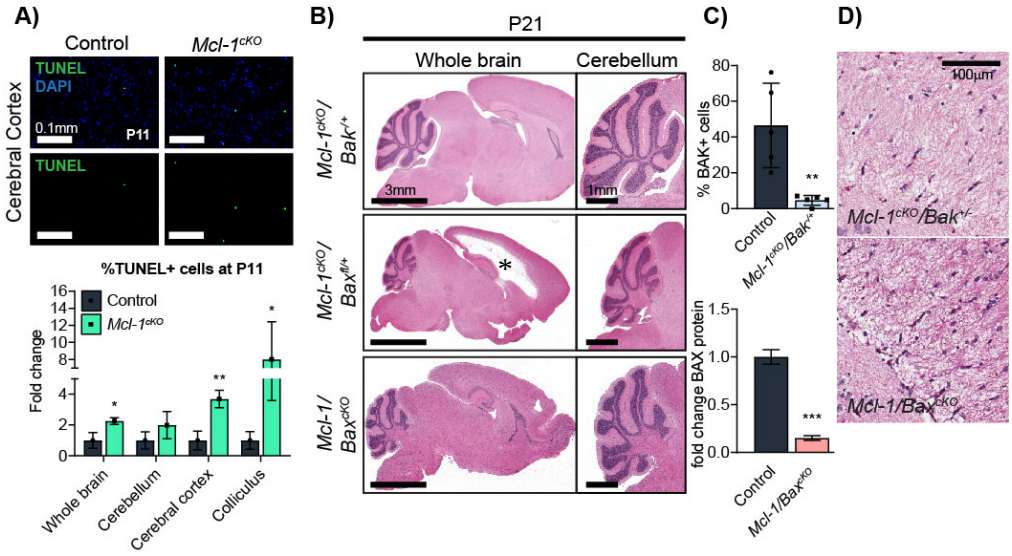

Figure 3. *Mcl-1* deletion causes white matter degeneration by increasing apoptosis. (**A**) TUNEL demonstrates increased cell death in *Mcl-1*^{cKO} brains. For cell counts, one sagittal section from each replicate was scanned at 20x and TUNEL+ cells were counted across the entire portion of each designated region that was contained within the section. (**B**) Representative H&E sections show that heterozygous *Bak* co-deletion and homozygous *Bax* co-deletion both rescue the white matter loss with ventricular enlargement (*) and cerebellar abnormalities caused by *Mcl-1* deletion. (**C**) Quantification of BAK immunohistochemistry in corpus callosum shows that heterozygous *Bak* deletion significantly reduces the

number of BAK+ cells. Quantification of western blot of whole cerebella shows that homozygous *Bax* deletion reduces BAX protein abundance. (**D**) Representative images of the corpus callosum in P14 mice of the indicated genotypes shows mild white matter rarefaction in *Mcl-1/Bax*^{dKO} mice, not seen in *Mcl-1*^{cKO}*/Bak*$^{+/-}$ mice. *, ** and *** denote $p<0.05$, $p<0.01$ and $p<0.001$ respectively, relative to controls.

Mcl-1-deleted mice with homozygous *Bax* co-deletion, with the genotype *hGFAP-Cre/Mcl1*$^{loxP/loxP}$*/Bax*$^{loxP/loxP}$ (*Mcl-1/Bax*^{dKO}) showed normal survival, similar to *Mcl-1*^{cKO}*/Bak*$^{-/+}$ mice. Compared to *Mcl-1*^{cKO} mice, *Mcl-1/Bax*^{dKO} mice showed greatly reduced neurologic deficits; however, we noted that by 200 days, *Mcl-1/Bax*^{dKO} showed a slight delay in movement on opening the cage that was not seen in *Mcl-1*^{cKO}*/Bak*$^{+/-}$ mice. The extensive white matter loss in *Mcl-1*^{cKO} mice was rescued in *Mcl-1/Bax*^{dKO} mice (Fig. 3B). Close examination of brain sections from *Mcl-1/Bax*^{dKO} mice, however, showed mild white matter loss (Fig. 3D). The rescued phenotypes of *Mcl-1*^{cKO}*/Bak*$^{-/+}$ and *Mcl-1/Bax*^{dKO} mice show that disrupting either *Bax* or *Bak* is sufficient to prevent the severe white matter degeneration that otherwise results from *Mcl-1* deletion, implicating apoptosis in the pathogenesis of the *Mcl-1*^{cKO} phenotype. The mild neurologic deficits and white matter loss in *Mcl-1/Bax*^{dKO} mice showed that co-deletion of *Bax* and *Bak* do not have identical effects in *Mcl-1*-deleted animals.

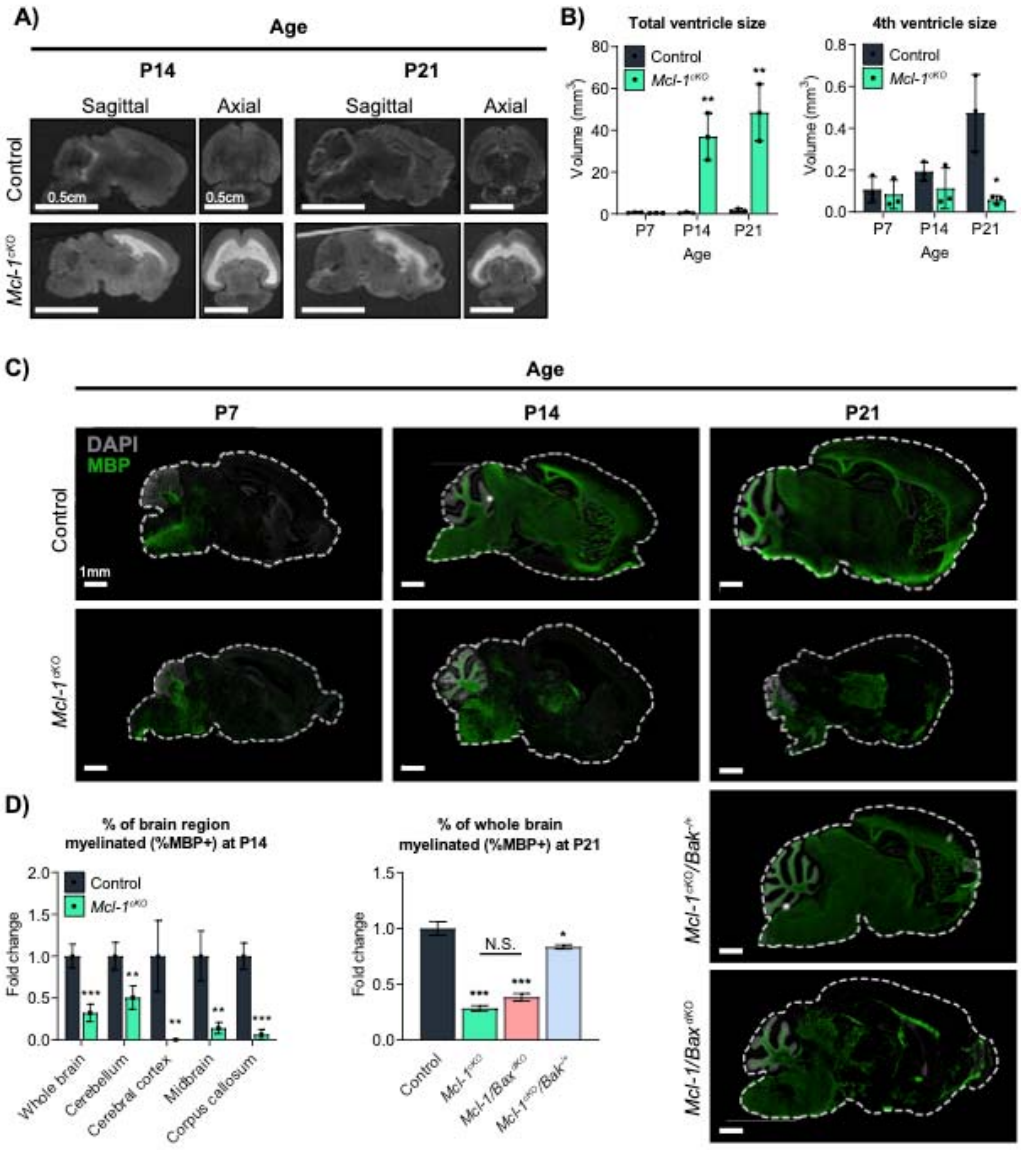

Figure 4. Abnormal neuroimaging and myelination in *Mcl-1*-deleted mice, with different rescue effects caused by co-deletion of *Bak* or *Bax*. (**A**) Representative MRIs show white matter hyperintensity in *Mcl-1*^{cKO} mice. (**B**) Total ventricular volume is abnormal in *Mcl-1*^{cKO} mice and increases from P7-P21, while the volume of the 4th ventricle decreases significantly by P21. (**C,D**) Representative images and quantitative analysis of MBP IHC show that myelination is markedly decreased in *Mcl-1*^{cKO} mice, rescued in *Mcl-1*^{cKO}*/Bak*$^{+/-}$ mice, and incompletely

rescued in *Mcl-1/Bax*^{dKO} mice. **(D)** Graphs show MBP+ area/total area within individual sections, normalized to the mean value in the control mice. *, ** and *** denote $p<0.05$, $p<0.01$ and $p<0.001$ respectively, relative to controls.

Mcl-1 deletion phenocopies human leukodystrophies

Leukoencephalopathies in patients produce characteristic MRI findings, including high water signal in white matter tracts (Vanderver et al., 1993), and the replacement of white matter by cerebrospinal fluid (van der Knaap et al., 1993). We analyzed whether *Mcl-1*^{cKO} mice showed similar white matter changes on MRI. Similar to VWMD patients, *Mcl-1*^{cKO} mice showed progressive ventriculomegaly (Fig. 4A). The increase in ventricle size was not evenly distributed, however, as the volume of the 4th ventricle was significantly smaller in *Mcl-1*^{cKO} mice at P21 (Fig. 4B). Increased lateral ventricles and reduced 4th ventricle was consistent with loss of periventricular cerebral white matter and an overall reduction in intracranial pressure, indicating hydrocephalus *ex vacuo*.

To determine whether myelination was disrupted in *Mcl-1*^{cKO} mice, we analyzed the distribution of Myelin Basic Protein (MBP). In control brains, the MBP+ area increased markedly from P7 to P14 (Fig. 4C). In contrast, myelination was delayed in *Mcl-1*^{cKO} brains, which showed significantly less MBP+ area at P14 in all brain regions analyzed (Fig. 4D).

Analysis of MBP+ area in *Mcl-1*-deleted mice with *Bax* or *Bak* co-deletions showed that myelination required MCL-1 specifically to regulate BAK. We compared brains in P21 animals, when normal brains show widespread myelination. Heterozygous *Bak* co-deletion largely rescued myelination in *Mcl-1*^{cKO}/*Bak*$^{+/-}$ mice. In these animals, MBP+ area was over 2-fold greater than in *Mcl-1*^{cKO} mice,

although we noted a small, statistically significant decrease in myelination compared to *Mcl-1* intact controls. Homozygous *Bax* deletion, however, did not rescue myelination in *Mcl-1/Bax*^{dKO} mice (Fig. 4D). The differential effects of *Bak* or *Bax* deletion on myelination support the interpretation that BAX and BAK act in cells with different functions, with both BAX and BAK affecting white matter maintenance, and only BAK affecting myelination.

Mcl-1 **deletion reduces oligodendrocyte and Bergmann glia populations**

To determine if impaired myelination in *Mcl-1*^{cKO} mice resulted from oligodendrocyte loss, we compared the numbers of cells expressing the oligodendrocyte marker SOX10 in *Mcl-1*^{cKO} and control mice (Fig. 5A). SOX10 marks the oligodendrocyte lineage from the initial fate commitment in oligodendrocyte precursors to the maturation of myelinating oligodendrocytes (Glasgow et al., 2014, Nishiyama et al., 2016); SOX10 cell counts thus reflect the total oligodendrocytic population across the differentiation spectrum. At P7, oligodendrocyte populations in *Mcl-1*^{cKO} mice were not significantly different from controls. By P14, *Mcl-1*^{cKO} mice showed significantly fewer SOX10+ cells in diverse brain regions (Fig. 5B), indicating a global decrease in oligodendrocytic cells. At P21, oligodendrocytic populations remained reduced in the cerebellum, corpus callosum, and superior colliculus, but were not statistically significantly reduced in the hippocampus and cerebral cortex, raising the possibility of a dynamic, homeostatic response in these gray matter regions.

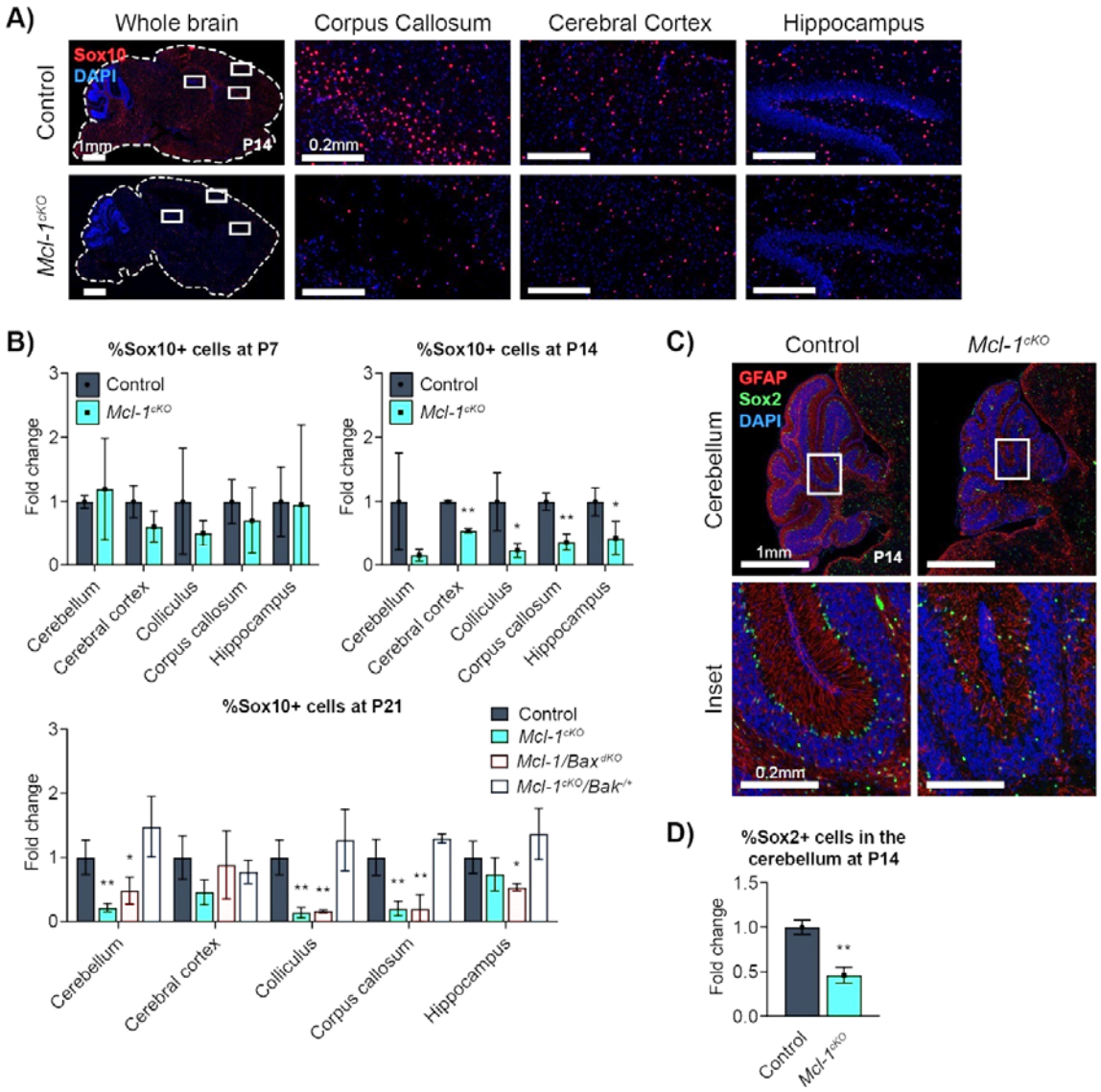

Figure 5. *Mcl-1* deletion causes loss of oligodendrocytes and Bergmann glia that is rescued with regional variation by co-deletion of *Bak* or *Bax*. (**A,B**) Representative images and quantification of SOX10 IHC in the indicated genotypes. (**C**) Representative immunofluorescence for GFAP and SOX2 IHC identify Bergmann glia in P14 mice of indicated genotypes. (**D**) SOX2+ cells are significantly reduced in *Mcl-1*^{cKO} mice. * and ** denote p<0.05 and p<0.01 respectively, relative to controls.

To determine if apoptosis mediates the decline in the oligodendrocyte populations in *Mcl-1*-deleted mice, we examined the effect of *Bax* or *Bak* co-deletion

in *Mcl-1*^{cKO}/*Bak*$^{+/-}$and *Mcl-1/Bax*^{dKO} mice. Heterozygous *Bak* co-deletion in *Mcl-1*^{cKO}/*Bak*$^{+/-}$ mice normalized oligodendrocyte population size, but homozygous *Bax* deletion in *Mcl-1/Bax*^{cKO} mice did not (Fig. 5B). *Bak* co-deletion thus rescued the effects of *Mcl-1* deletion on white matter volume, myelination, and total oligodendrocyte populations. In contrast, *Bax* co-deletion rescued only white matter volume, but myelination and oligodendrocyte numbers remained affected in *Mcl-1/Bax*^{dKO} mice. The discordant effects of *Bak* and *Bax* co-deletions suggest that MCL-1 discretely controls BAK-dependent apoptosis or BAX-dependent apoptosis in different types of white matter cells.

In contrast to the discordant effects of *Bax* and *Bak* co-deletions in oligodendrocytes, Bergmann glia were rescued by either co-deletion. We examined Bergmann glia because of their known involvement in VWMD (Dooves et al., 2016), and because of the migration abnormalities in *Mcl-1*^{cKO} mice, as Bergmann glia guide cerebellar granule neuron progenitors as they migrate to the internal granule cell layer to become cerebellar granule neurons (Hatten, 1990, Rakic, 1971). We identified Bergmann glia as cells with SOX2+ nuclei and GFAP+ processes (Fig. 5C). At P7, the numbers of Bergmann glia in *Mcl-1*^{cKO} were similar to control mice (data not shown), but by P14, the Bergmann glia populations in *Mcl-1*^{cKO} mice were significantly reduced (Fig. 5D). The loss of Bergmann glia during the period of CGN migration account for the observed cerebellar migration defects. Co-deletion of either one copy of *Bak* in *Mcl-1*^{cKO}/*Bak*$^{+/-}$ mice or both copies of *Bax* in *Mcl-1/Bax*^{dKO} mice was sufficient to rescue cerebellar migration, indicating that MCL-1 functions in Bergmann glia to restrict an apoptotic program that requires both BAX AND BAK in order to drive cell death.

Mcl-1 **deletion alters the astrocytic populations**

While *Mcl-1*^{cKO} mice contained fewer Bergmann glia, we noted increased numbers of GFAP+ astrocytic processes throughout the brain, that was most conspicuous in the relatively hypocellular molecular layer of the cerebellum (Fig. 6A). To determine if this increase in GFAP+ cells indicated an increase in the total number of astrocytes or an increase in the fraction of astrocytes expressing GFAP, we compared the number of cells expressing the astrocytic nuclear marker SOX9 in *Mcl-1*^{cKO} mice and controls (Fig. 6B). SOX9+ cells were not significantly increased in *Mcl-1*^{cKO} mice in any brain region at either P7 or P14, and rather were decreased in the corpus callosum at P14 (Fig. 6B,C). The increase in GFAP+ processes in *Mcl-1*^{cKO} mice without the increase in SOX9+ cells shows the *Mcl-1* deletion did not increase the total astrocyte population, but rather increased the fraction of astrocytes expressing GFAP, indicating a reactive response to injury (Eddleston and Mucke, 1993, Dahl and Bignami, 1974).

The intermediate filament protein NESTIN is known to be up-regulated in reactive astrocytes (Tamagno and Schiffer, 2006, Schmidt-Kastner et al., 2005, Sahin Kaya et al., 1999, Clarke et al., 1994), and prior studies report increased Nestin-expressing astrocytes in white matter from humans with VWMD (Bugiani et al., 2011). Similarly, *eIF2B5* $^{R191H/R191H}$ mice show increased astrocytes expressing both Nestin and GFAP in the corpus callosum, compared to wildtype controls (Dooves et al., 2016, Geva et al., 2010). To determine if *Mcl1*-deleted mice also showed similar astrocytic changes, we compared Nestin+/GFAP+ populations in

P14 *Mcl-1*^{cKO} mice and controls (Fig. 6D). *Mcl-1*^{cKO} mice demonstrated increased fractions of Nestin+/GFAP+ cells in the corpus callosum (Fig 5E), with a trend toward increased fractions in other white matter regions, consistent with astrocytic changes in VWMD patients and *eIF2B5* $^{R191H/R191H}$ mice. *Mcl-1*^{cKO} mice thus recapitulated both the astrocytic and oligodendrocytic abnormalities seen in VWMD in patients and the VWMD mouse models.

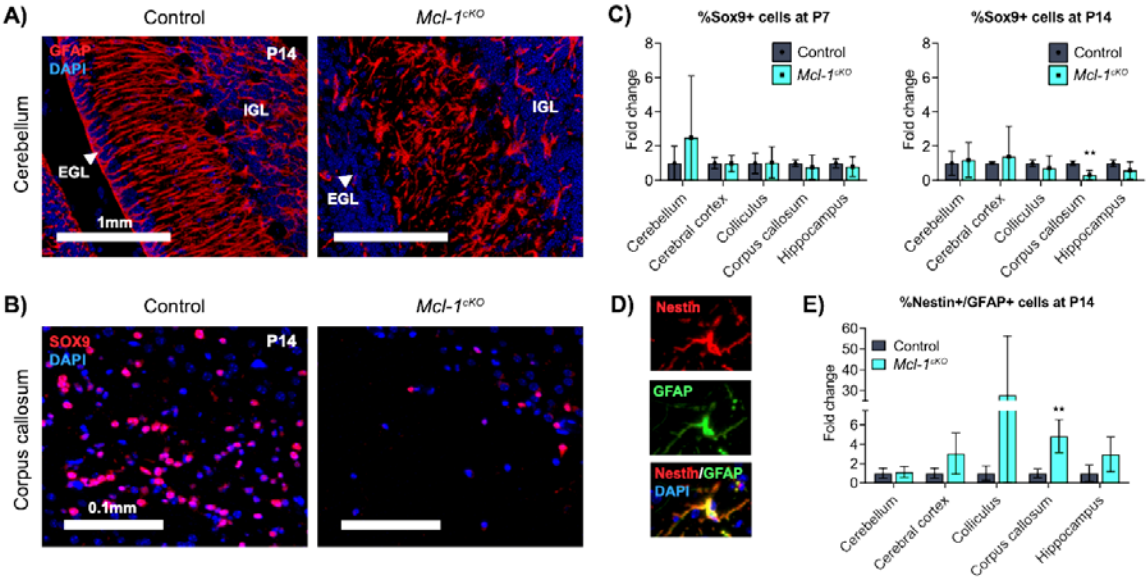

Figure 6. Mcl-1 deletion causes reactive astrocytosis. (**A**) Representative GFAP IHC in sections of P14 cerebella in the indicated genotypes shows Bergmann glia processes in the control mice that are absent in the *Mcl-1*^{cKO}, and numerous astrocyte processes in the *Mcl-1*^{cKO} mice. (**B**) Representative SOX9 IHC in sections of P14 corpus callosum in the indicated genotypes show a significant decrease of SOX9+ cells in the *Mcl-1*^{cKO} mice. (**C**) Quantification of SOX9 IHC at the indicated ages and genotypes, showing that astrocyte numbers are not increased in *Mcl-1*^{cKO} mice. (**D,E**) Nestin/GFAP IHC, with representative images and quantification in the indicated genotypes. * and ** denote $p<0.05$ and $p<0.01$ respectively, relative to controls.

Mcl-1 deletion causes neuroinflammation

Brains of *Mcl-1*^{cKO} mice contained increased cells expressing the myeloid marker IBA1 (Fig. 7A), indicating microglial activation (Ito et al., 1998, Imai et al., 1996). The microglial changes in *Mcl-1*^{cKO} mice began later than the astrocytic and oligodendrocytic changes, beginning at the corpus callosum at P14; by P21, *Mcl-1*^{cKO} mice showed increased IBA+ cells in diverse brain regions (Fig. 7B). The increased IBA1+ microglia in *Mcl-1*^{cKO} mice demonstrates a non-cell autonomous effect in which *Mcl-1* deletion in the glio-neuronally restricted GFAP lineage induced inflammatory changes in myeloid cells.

Co-deletion of either *Bak* or *Bax* prevented microgliosis in different brain regions. Heterozygous co-deletion of *Bak* in *Mcl-1*^{cKO}*; Bak*$^{+/-}$ mice significantly reduced IBA1+ cells in the cerebellum, cerebral cortex, colliculus, and corpus callosum, relative to *Mcl-1*^{cKO} mice. In contrast, homozygous co-deletion of *Bax* in *Mcl-1*$^{/}$*Bax*^{dKO} mice showed a significant decrease in IBA1+ cells in the hippocampus, relative to both *Mcl-1*^{cKO} and *Mcl-1*^{cKO}*/Bak*$^{+/-}$ mice (Fig. 7B). The rescue of neuro-inflammation by co-deletion of *Bax* or *Bak* implicates increased regional apoptosis as the cause of inflammation, while the region-specific pattern of rescue further supports the conclusion that white matter cells in different areas of the brain alternatively regulate apoptosis through interactions of MCL-1 with either BAX or BAK.

Decreased brain MCL-1 protein in a VWMD mouse model

Based on the similarity of the *Mcl-1*^{cKO} phenotype to VWMD, the role of the ISR in VWMD, and the regulation of MCL-1 abundance by the ISR, we investigated whether changes in MCL-1 protein might mediate the effect of mutant eIF2B on glial cells. To begin to test this possibility, we compared MCL-1 abundance in brain

lysates from wildtype and *eIF2B5* $^{R132H/R132H}$ mice at 7 and 10 months old (Fig. 7C). We found that by 10 months, *eIF2B5* $^{R132H/R132H}$ mice expressed reduced MCL-1 protein in the brain, indicating that the *eIF2B5* $^{R132H/R132H}$ mutation results in reduced MCL-1 expression over time. In *eIF2B5* $^{R132H/R132H}$ mice, the temporal course of reduced brain MCL-1 protein correlated with the development of VWMD symptoms. Thus, along with our finding that MCL-1 deficiency in *Mcl-1*^{cKO} mice was sufficient to cause a VWMD phenotype, we found declining MCL-1 expression in *eIF2B5* $^{R132H/R132H}$ mice that model VWMD.

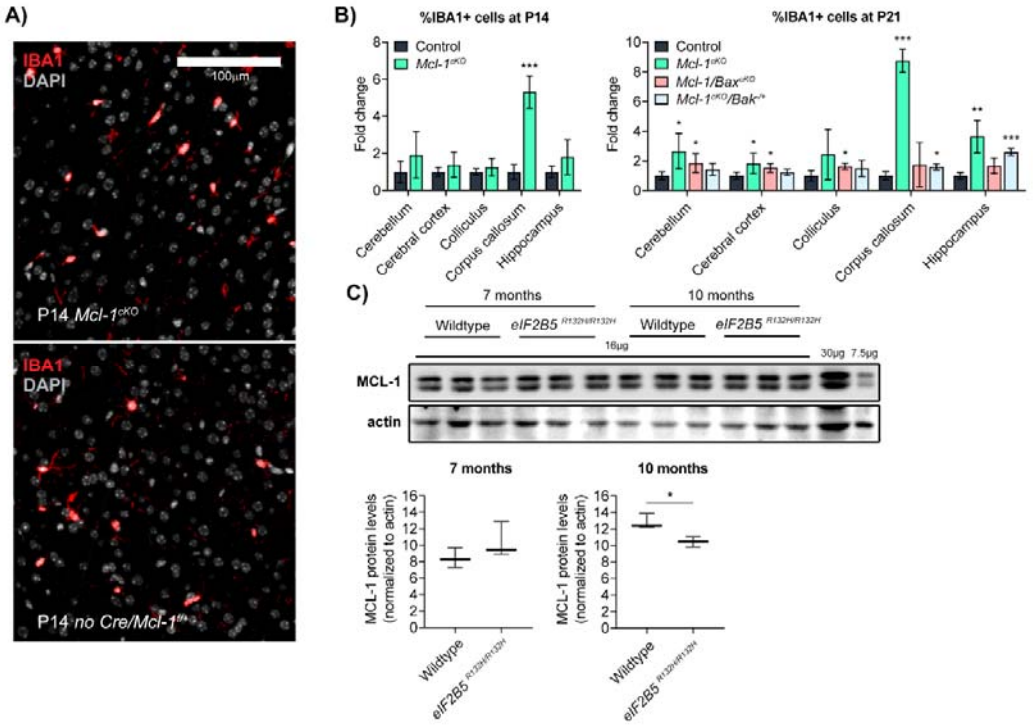

Figure 7. Progressive neuroinflammation in *Mcl-1*^{cKO} mice and reduced MCL-1 protein in mice with VWMD. (**A,B**) IBA1 IHC, with representative images and quantification in the indicated genotypes, showing a progressive increase in microglia in *Mcl-1*^{cKO} mice, beginning in the corpus callosum at P14 and expanding to include diverse regions by P21. Co-deletion of *Bak* or *Bax* variably rescue microgliosis with different effects in different regions. *, ** and *** denote p<0.05,

p<0.01 and p<0.001 respectively, relative to controls. (**C**) Western blot comparing MCL-1 protein abundance in brain lysates of 7- and 10-months old WT and *eIF2B5*$^{R132H/R132H}$ mice, demonstrating reduced MCL-1 in 10-month old mutant mice. * denotes p<0.03, relative to controls.

Discussion

Our data show that conditional deletion of anti-apoptotic *Mcl-1* in neuro-glial stem cells results in a progressive encephalopathy with post-natal white matter degeneration. While prior studies have shown increased apoptosis in embryonic and adult neural progenitors resulting from *Mcl-1* deletion (Fogarty et al., 2019, Hasan et al., 2013, Malone et al., 2012), our data show that brain-wide *Mcl-1* deletion produces postnatal brain white matter degeneration that closely resembles the human leukodystrophy VWMD. Although MCL-1 mutations have not been described in any human leukodystrophy, the mechanisms of white matter injury in human leukodystrophies are unresolved. Our studies show that disruption of MCL-1-dependent apoptosis control in the entire brain specifically impacts white matter and is sufficient to produce leukodystrophy.

The *Mcl-1*^{cKO} phenotype presented striking similarities to human leukodystrophies, and most specifically to VWMD. Brain function and white matter appeared normal in *Mcl-1*^{cKO} mice until after P7, when mice showed motor and sensory impairment, delayed myelination, and rarefaction of the periventricular white matter and corpus callosum, eventually leading to white matter loss and hydrocephalus *ex vacuo*. Similar to VWMD, mature myelinating oligodendrocytes were markedly reduced, Bergmann glia of the cerebellum were also affected, and astrocytes showed reactive changes that are also seen in astrocytes in VWMD, including up-regulation of GFAP and NESTIN. The similarity of the *Mcl-1*^{cKO} and

VWMD phenotypes, including the overall histopathology of vanishing white matter and the specific loss of terminally differentiated oligodendrocytes and Bergmann glia, show that *eIF2B* mutations and *Mcl-1* deletion affect specific cells of the brain in a similar manner.

Taken together, reduced MBP and SOX10 demonstrate that within global oligodendrocyte depletion of *Mcl-1*^{cKO} mice, mature, myelinating oligodendrocytes are particularly affected. Studies in VWMD patients and mouse models show that while mature oligodendrocyte populations are reduced, immature oligodendrocyte precursors may actually be increased (Herrero et al., 2019, Bugiani et al., 2013). A similar increase in immature oligodendrocytes may occur in the *Mcl-1*^{cKO} mice and would not be inconsistent with the observed overall reductions in SOX10+ brain cells and brain myelination.

The similarity of the *Mcl-1*^{cKO} phenotype to VWMD raises the possibility that reduced MCL-1 protein abundance specifically contributes to VWMD pathology. The known activation of the ISR in VWMD (Abbink et al., 2019, Kantor et al., 2005) and the suppression of MCL-1 translation by the ISR together provide a potential molecular mechanism to link the *Mcl-1*^{cKO} phenotype to VWMD. Consistent with this proposed mechanism, we found reduced MCL-1 protein in *eIF2B5* $^{R132H/R132H}$ mice, which correlated with the development of white matter pathology. While studies in patient-derived samples could potentially test whether MCL-1 abundance is altered in VWMD patients, these studies would require samples that preceded fulminant white matter loss, in order to include oligodendrocyte populations that may be lost through apoptosis. Our data show that MCL-1 deficiency is sufficient to reproduce

the VWMD phenotype in mice. Studies of *Bax* and *Bak* deletion in *eIF2B5* $^{R132H/R132H}$ mice would allow testing of whether apoptosis is required for VWMD.

The rescue of the *Mcl-1*^{cKO} phenotype by co-deletion of *Bak* or *Bax* implicate apoptosis in the causation of white matter loss in *Mcl-1*^{cKO} mice. We previously found that conditional *Mcl-1* deletion in cerebellar granule neuron progenitors does not produce a phenotype of gray matter loss as these cells regulate BAX via the homologous anti-apoptotic protein BCL-xL *(Crowther et al., 2013)*. The specific dependencies of different cell types on different anti-apoptotic factors is also seen outside the nervous system, as in the myeloid lineage where neutrophils undergo spontaneous apoptosis when *Mcl-1* is deleted, but macrophages survive (Dzhagalov et al., 2007). Different cell types within broad lineages may thus require different anti-apoptotic family proteins to regulate apoptosis, and the survival of neurons and astrocytes in *Mcl-1*^{cKO} mice shows that within the broad lineage derived from glio-neuronal stem cells, MCL-1 protein is specifically required by a subset of cells at some point along the more narrow lineage of the oligodendrocytes.

In addition to demonstrating the requirement for apoptosis in white matter degeneration in *Mcl-1*^{cKO} mice, the *Bax* and *Bak* rescue studies demonstrate that myelination defects and white matter loss can be dissociated. Co-deletion of *Bak* rescued both myelination, oligodendrocyte populations, and white matter loss. In contrast co-deletion of *Bax* reduced white matter loss without rescuing myelination and oligodendrocyte populations. These differences show that different cell types that can be differentiated by their apoptosis regulation contribute to different aspects of the *Mcl-1*^{cKO} phenotype.

The possibility that BAX and BAK act in different cells with different sensitivities does not require differential expression patterns. For example, prior studies show that both BAX and BAK can drive apoptosis in cerebellar granule neuron progenitors, but under different conditions. BAX-dependent apoptosis in these cells can be engaged either by radiation-induced DNA damage (Chong et al., 2000), or by chromosomal fragmentation in the setting of *Atr* deletion (Lang et al., 2016). In contrast, BAK-dependent apoptosis is not engaged by radiation, as radiation induced apoptosis is blocked by *Bax* deletion(Crowther et al., 2013, Chong et al., 2000); BAK-dependent apoptosis requires the more intense trigger of *Atr* deletion and resulting chromosomal fragmentation (Lang et al., 2016). These prior studies show that cells in the CNS that express both BAX and BAK can show different mechanisms and sensitivities for triggering BAX-dependent or BAK-dependent apoptosis. Similarly, specific subsets of glia may regulate BAX-dependent and BAK-dependent apoptosis through different mechanisms, with different, cell-type specific sensitivities and dependencies on MCL-1.

The rescue myelination by co-deletion of *Bak* but not *Bax* shows that myelinating oligodendrocytes or their precursors regulate apoptosis specifically through MCL-1:BAK interactions. The different rescue pattern with *Bax* co-deletion, which prevented white matter degeneration without normalizing myelination, shows that a different type of cell regulates white matter loss and requires both BAK and BAX to be present for *Mcl-1* deletion to produce phenotype changes. Clearly, diverse cell types are affected in both *Mcl-1*^{cKO} mice and VWMD patients (Bugiani et al., 2018, Zhou et al., 2019). Our genetic rescue studies show that different types of glial cells depend on MCL-1 to regulate different pro-apoptotic proteins, and that loss of this regulation in different types of cells reproduces different aspects of the

overall pathology. The loss of multiple subsets of glial cells may similarly contribute to different aspects of the overall VWMD phenotype.

While multiple mutations can cause leukodystrophies, for many of these genetic diseases, the mechanistic steps from mutation to white matter loss remain to be specified in detail. Our findings that MCL-1 deletion in neuro-glial stem cells produces white matter degeneration, and that this degeneration is rescued by co-deletion of *Bax* or *Bak* implicates the process of apoptosis in the causation of leukodystrophy. Moreover, our rescue experiments show that apoptosis in multiple cell types derived from neuro-glial stem cells contribute to different aspects of white matter pathology. Treatments that inhibit the intrinsic apoptotic pathway in the postnatal brain may provide an avenue for reducing the impact of diverse leukodystrophies.

Acknowledgments: supported by R01NS088219 (TRG), R01NS102627 (TRG), and R01NS1062 (TRG), T32CA071341 (AHC), 4R00CA178190 (VG), R35GM128915 (VG), and R21CA227483 (VG), U54 HD079124 (VDM,SM).

Author Contributions: Conceptualization, T.R.G. and V.G.; Methodology, A.H.C., V.D.M., S.M, T.R.G., V.G. and O.E-S.; Investigation, A.H.C, V.D.M., A.R., L.A.A., M.H.,; Writing – Original Draft, A.H.C. and T.R.G.; Writing – Review & Editing, O.E-S., S.M., V.G. and T.R.G; Funding Acquisition, V.G., and T.R.G.;; Resources, O.E-S., V.G., and T.R.G.; Supervision, S.M.,O.E-S., V.G., and T.R.G.

Methods

Mice

We generated *Mcl-1*^{cKO} mice, by crossing *GFAP-Cre* mice (Jackson Labs, stock # 004600) with *Mcl-1*$^{LoxP/LoxP}$ mice (Dzhagalov et al., 2007), generously shared by Dr.

You-Wen He. We interbred GFAP-Cre, *Mcl-1*$^{loxP/loxP}$, and *Bax*$^{LoxP/LoxP}$*/Bak*$^{-/-}$ (Jackson Labs, stock # 006329) to generate *Mcl-1;Bax*^{dKO}, *Mcl-1;Bak*^{dKO}, and various heterozygous controls. We generated *EMX1-Cre/Mcl-1*$^{loxP/loxP}$ mice by breeding *EMX1-Cre* mice, generously provided by Dr. William Snide, into the *Mcl-1 f/f* line. All mice were of species *Mus musculus* and crossed into the C57BL/6 background through at least five generations. All animal studies were carried out with the approval of the University of North Carolina Institutional Animal Care and Use Committee under protocols (19-099).

Wild type (C57BL/6 strain) and *eIF2B5*$^{R132H/R132H}$ mice (Geva et al., 2010) were generated, bred, and housed in Tel Aviv University animal facility (Lab Products Inc., Seaford, DE, USA). All experimental procedures were approved by the Tel Aviv University Animal Care Committee according to national guidelines (permit #04-17-022). Breeding and genotyping were performed as previously described. (Geva et al., 2010) Each generation was established by back cross of homozygous *eIF2B5*$^{R132H/R132H}$ mice with WT C57BL/6J (Harlan Labs, Jerusalem, Israel) to prevent genetic drift.

Histology and immunohistochemistry (IHC)

Mouse brains were processed and immunostained as previously described (Ocasio et al., 2019, Tech et al., 2017, Lang et al., 2016, Crowther et al., 2016). Primary antibodies used were: BAK diluted 1:200 (Cell Signaling, #12105), MBP diluted 1:1000 (Abcam, #ab7349), SOX10 diluted 1:100 (Santa Cruz, #sc-17342), cleaved-Caspase 3 (cC3) diluted 1:400 (Biocare Medical, #CP229C), glial fibrillary acidic protein (GFAP) diluted 1:2000 (Dako, Z0334), SOX2 1:200 (Cell Signaling, #4900S), SOX9 1:200 (R&D Systems, #AF3075), NESTIN 1:500 (Cell Signaling,

#4760), IBA1 1:2000 (Wako Chemicals, #019-19741). Stained images were counterstained with DAPI, digitally imaged using an Aperio Scan Scope XT (Aperio) and subjected to automated cell counting using Tissue Studio (Definiens).

Magnetic resonance imaging

For MRI studies, brains from P7, P14, and P21 mice were harvested and fixed in 4% formaldehyde in PBS for 48hrs, then transferred to PBS. Brains were then embedded in 2% agarose in 15mL plastic vials and imaged in pairs as previously described (Williams et al., 2015).

Western blot

Whole brains or cerebella were harvested and homogenized in lysis buffer (Cell Signaling, #9803). Lysate protein concentrations were quantified using a bicinchoninic acid (BCA) protein assay kit (Thermo scientific, #23225). Equal total protein concentrations were resolved on SDS-polyacrylamide gels (BioRad, # 4561105, # 4568094) and transferred onto polyvinylidene difluoride membranes. Membranes were blotted using a SNAP i.d. 2.0 Protein Detection System (Millipore). Membranes were imaged using a chemiluminescent SuperSignal West Femto Maximum Sensitivity Substrate (34095, Thermo Fisher Scientific) and the C-DiGit blot scanner (LI-COR Biosciences). Signal was quantified using the Image Studio Lite software (LI-COR). The following antibodies were used for western blot: MCL-1 (Cell Signaling, #94296; 1:500 dilution), BAX (Cell Signaling, #14796; 1:500 dilution), β-actin (Cell Signaling, #3700; 1:5000 dilution), Actin (Sigma #A3853; 1:240000 dilution), Anti-rabbit IgG, HRP-linked antibody (Cell Signaling, #7074; 1.5:1000 dilution), Anti-mouse IgG, HRP-linked antibody (Cell Signaling, #7076;

1.5:1000 dilution). For the eIF2B5$^{R132H/R132H}$ studies, cerebrums were harvested from 7 and 10 month old mice and protein was extracted using a lysis buffer containing 1% triton, 0.5% NaDOC, 0.1% SDS, 50 mM Tris pH 8, 100 mM NaCl, 10 mM β-glycerophosphate, 5 mM NaF, 1 mM DTT, 1 mM vanadate, and EDTA-free complete TM protease inhibitor cocktail (#11-836-170-001; ROCHE). Protein was quantified using a BCA protein assay kit (#23227 Pierce), diluted in 1X sample buffer (0.05 M HEPES pH 7.4, 2% (w/v) SDS, 10% (v/v) Glycerol, traces of Bromophenol Blue, 100 mM Dithiothreitol (DTT)), and separated on a 10% SDS-PAGE gel. Blots were imaged using an AI600 Imager (Amersham) and quantified by ImageQuant TL (GE Healthcare, Pittsburgh, PA, United States).

Behavioral studies

Animals included. Subjects were *Mcl-1^{cKO}* mice or littermate controls with intact Mcl-1, including genotypes Mcl1$^{f/+}$ without Cre, Mcl1$^{f/f}$ without Cre, and Gfap-Cre/Mcl1$^{f/+}$. A total of 8 litters were needed to generate all of the replicates. Day of birth was considered postnatal day 0 (P0). Subject numbers at the beginning of the study (P7) were 13 (21%) *Mcl-1^{cKO}* and 48 (79%) control. All litters completed the first 2 weeks of testing. Three litters (n=23) were removed from the study for histology assays during the third week of testing: one on P15, after the second open field test; one on PD16, after the first acoustic startle test; and one on P21, after the tail suspension test.

Behavioral testing regimen

Developmentally-calibrated behavioral tests: For motor tests at P7, mice were removed from the home cage and maintained in a beaker warmed to 35°C. Mice

were then subjected to the neurobehavioral negative geotaxis, righting, and open field tests, adapted from published studies (Cheh et al., 2006).

Negative geotaxis. A 20 cm × 20 cm screen with 0.5 cm wire mesh squares was set at a 25° angle. Each pup was placed downward on the screen with its head facing toward the bottom, allowed to grip the mesh, and then released. The time it took for each pup to turn 180° (head and upper torso vertical), was recorded, with a 30 s maximum and each pup was tested 3 times.

Righting. Each pup was placed onto its back on a flat Plexiglas surface. The experimenter gently held the pup in place for 2 s and then released it. The latency to righting (all 4 feet on the ground) was timed, with a maximum of 30 s.

Open field activity and pivoting. Each pup was placed into the center of a Plexiglas chamber (PhenoTyper; 30.5 cm × 30.5 cm × 43.5 cm; Noldus Information Technology, Wageningen, The Netherlands). A dim yellow light (30 lx) at the top of the PhenoTyper box was illuminated throughout the 3 min trial. Measures were taken of distance traveled and time in the center region (4 cm × 4 cm square in the center of the arena) by an image-tracking system (EthoVision, Noldus Information Technology). In addition, the experimenter recorded the number of vertical rearing movements and number of pivots (circling or lateral movement, as opposed to forward locomotion).

Each mouse was screened through the 3 assays in the order presented here. After finishing the neonatal motor screen, each pup was weighed, marked with a non-toxic Sharpie, and placed back into the warm beaker. The litter was returned to the home cage after all pups had been tested.

Open field activity at P14 and P19. Additional open field activity tests were performed at P14 and P19. The distance traveled, the number of vertical rearing movements, and time spent in the center region was recorded in each 10 min test.

Acoustic startle responses. This test was used to assess auditory function, reactivity to environmental stimuli, and sensorimotor gating. Mice were evaluated at 2 time points, P14 and P21. The procedure was based on the reflexive whole-body flinch, or startle response, that follows exposure to the acoustic stimuli. Measures were taken of startle magnitude and prepulse inhibition, which occurs when a weak stimulus leads to a reduced startle in response to a subsequent louder noise.

Mice were placed into individual Plexiglas cylinders within larger, sound-attenuating chambers. Each cylinder was seated upon a piezoelectric transducer, which allowed vibrations to be quantified and displayed on a computer (San Diego Instruments SR-Lab system). The chambers included a ceiling light, fan, and a loudspeaker for the acoustic stimuli. Background sound levels (70 dB) and calibration of the acoustic stimuli were confirmed with a digital sound level meter (San Diego Instruments). Each session began with a 5-min habituation period, followed by 42 trials of 7 different types: no-stimulus (NoS) trials, trials with the acoustic startle stimulus (AS; 40 msec, 120 dB) alone, and trials in which a prepulse stimulus (20 msec; either 74, 78, 82, 86, or 90 dB) occurred 100 ms before the onset of the startle stimulus. Measures were taken of the startle amplitude for each trial across a 65-msec sampling window, and an overall analysis was performed for each subject's data for levels of prepulse inhibition at each prepulse sound level (calculated as 100 - [(response amplitude for prepulse stimulus and startle stimulus together / response amplitude for startle stimulus alone) x 100].

Limb clasping. At PD18-21, a subset of mice (n=39) was assessed for limb clasping during a tail-suspension test. Each mouse was lifted by the base of the tail, and suspended above cage bedding for 15 sec, with ventral (stomach) side facing the experimenter. Response to tail suspension was coded using the following scoring system:

Forepaw movement

-2 = paws are clasped together, little movement, may be drawn up against chest

0 = paws move quickly in periodic flailing or kicking motions

2 = vigorous movement, may resemble rapid digging

Hindlimb placement and movement

-4 = both hindlimbs are retracted inwards toward abdomen, with little movement

-2 = hindlimbs are partially or intermittently retracted inwards toward abdomen

0 = hindlimbs are splayed outward from the abdomen. Moderate kicking behavior

2 = vigorous rapid kicking

Statistical analysis of behavioral tests

All testing was conducted by experimenters blinded to mouse genotype. Statview (SAS, Cary, NC) was used for data analyses. To reduce the number of *Mcl-1*^{cKO} subjects required, behavioral data from males and females were combined. One-way or repeated measures analysis of variance (ANOVA) were used to determine effects of genotype. Post-hoc analyses were conducted using Fisher's Protected

Least Significant Difference (PLSD) tests following a significant ANOVA F value. For all comparisons, significance was set at $p<0.05$.

Supplementary Figures

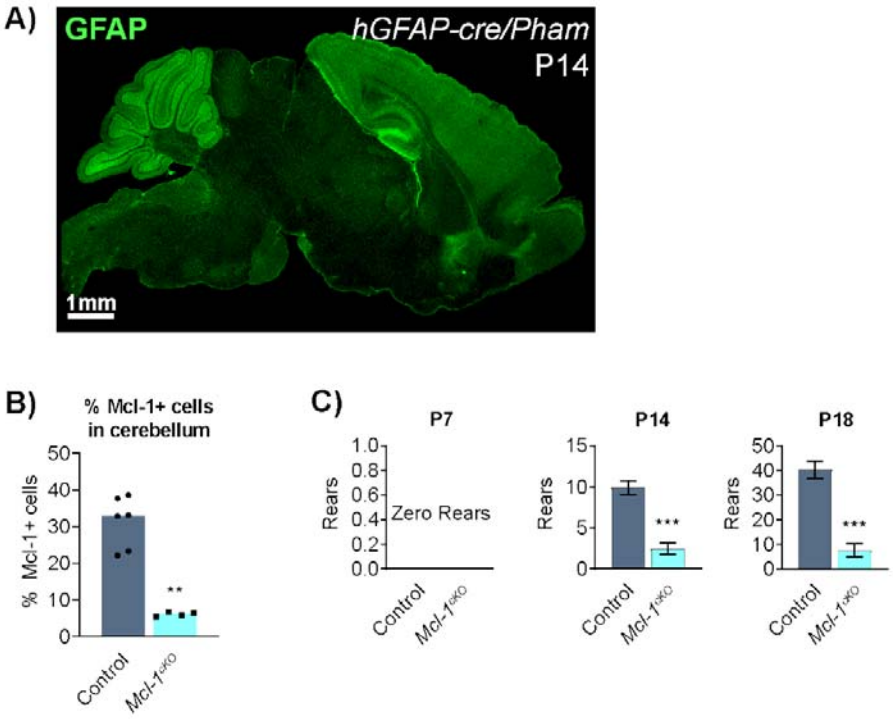

Supplementary Figure 1. *hGFAP-Cre* conditionally deletes *Mcl-1* in regions throughout the brain. A) *hGFAP-Cre* induces expression of the fluorescent reporter DENDRA2 in *hGFAP-cre/Pham* mice, indicating regions of GFAP expression. *hGFAP-Cre* targets cells in diverse regions throughout the brain, including the cerebellum, hippocampus, and cortex. **B)** MCL-1 protein levels are significantly reduced in cerebella of *Mcl-1*^{cKO} mice. **C)** *Mcl-1*^{cKO} mice displayed decreased rearing at both P14 and P18.

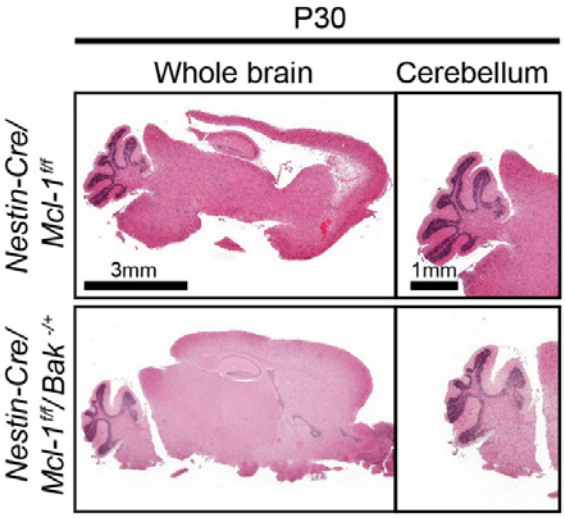

Supplementary Figure 2. *Nestin-Cre/Mcl-1$^{f/f}$* mice develop white matter degeneration similar to that of *Mcl-1^{cKO}* mice. Similar to GFAP-Cre, Nestin-Cre targets cells of both the neural and glial lineage. Brains harvested from *Nestin-Cre/Mcl-1$^{f/f}$* mice showed ventricular dilation and white matter rarefaction by P30. Deletion of one copy of *Bak* rescued this phenotype in *Nestin-Cre/Mcl-1$^{f/f}$/Bak $^{-/+}$* mice.

References

ABBINK, T. E. M., WISSE, L. E., JAKU, E., THIECKE, M. J., VOLTOLINI-GONZALEZ, D., FRITSEN, H., BOBELDIJK, S., TER BRAAK, T. J., POLDER, E., POSTMA, N. L., BUGIANI, M., STRUIJS, E. A., VERHEIJEN, M., STRAAT, N., VAN DER SLUIS, S., THOMAS, A. A. M., MOLENAAR, D. & VAN DER KNAAP, M. S. 2019. Vanishing white matter: deregulated integrated stress response as therapy target. *Ann Clin Transl Neurol,* 6**,** 1407-1422.

BUGIANI, M., BOOR, I., POWERS, J. M., SCHEPER, G. C. & VAN DER KNAAP, M. S. 2010. Leukoencephalopathy with vanishing white matter: a review. *J Neuropathol Exp Neurol,* 69**,** 987-96.

BUGIANI, M., BOOR, I., VAN KOLLENBURG, B., POSTMA, N., POLDER, E., VAN BERKEL, C., VAN KESTEREN, R. E., WINDREM, M. S., HOL, E. M., SCHEPER, G. C., GOLDMAN, S. A. & VAN DER KNAAP, M. S. 2011. Defective glial maturation in vanishing white matter disease. *J Neuropathol Exp Neurol,* 70**,** 69-82.

BUGIANI, M., POSTMA, N., POLDER, E., DIELEMAN, N., SCHEFFER, P. G., SIM, F. J., VAN DER KNAAP, M. S. & BOOR, I. 2013. Hyaluronan accumulation and arrested oligodendrocyte progenitor maturation in vanishing white matter disease. *Brain,* 136**,** 209-22.

BUGIANI, M., VUONG, C., BREUR, M. & VAN DER KNAAP, M. S. 2018. Vanishing white matter: a leukodystrophy due to astrocytic dysfunction. *Brain Pathol,* 28**,** 408-421.

CHEH, M. A., MILLONIG, J. H., ROSELLI, L. M., MING, X., JACOBSEN, E., KAMDAR, S. & WAGNER, G. C. 2006. En2 knockout mice display neurobehavioral and neurochemical alterations relevant to autism spectrum disorder. *Brain Res,* 1116**,** 166-76.

CHONG, M. J., MURRAY, M. R., GOSINK, E. C., RUSSELL, H. R. C., SRINIVASAN, A., KAPSETAKI, M., KORSMEYER, S. J. & MCKINNON, P. J. 2000. Atm and Bax cooperate in ionizing radiation-induced apoptosis in the central nervous system. *Proceedings of the National Academy of Sciences,* 97**,** 889-894.

CLARKE, S. R., SHETTY, A. K., BRADLEY, J. L. & TURNER, D. A. 1994. Reactive astrocytes express the embryonic intermediate neurofilament nestin. *Neuroreport,* 5**,** 1885-8.

CROWTHER, A. J., GAMA, V., BEVILACQUA, A., CHANG, S. X., YUAN, H., DESHMUKH, M. & GERSHON, T. R. 2013. Tonic activation of Bax primes neural progenitors for rapid apoptosis through a mechanism preserved in medulloblastoma. *The Journal of neuroscience : the official journal of the Society for Neuroscience,* 33**,** 18098-108.

CROWTHER, A. J., OCASIO, J. K., FANG, F., MEIDINGER, J., WU, J., DEAL, A. M., CHANG, S. X., YUAN, H., SCHMID, R., DAVIS, I. & GERSHON, T. R. 2016. Radiation Sensitivity in a Preclinical Mouse Model of Medulloblastoma Relies on the Function of the Intrinsic Apoptotic Pathway. *Cancer Res,* 76**,** 3211-23.

DAHL, D. & BIGNAMI, A. 1974. Heterogeneity of the glial fibrillary acidic protein in gliosed human brains. *J Neurol Sci,* 23**,** 551-63.

DOOVES, S., BUGIANI, M., POSTMA, N. L., POLDER, E., LAND, N., HORAN, S. T., VAN DEIJK, A. L., VAN DE KREEKE, A., JACOBS, G., VUONG, C., KLOOSTER, J., KAMERMANS, M., WORTEL, J., LOOS, M., WISSE, L. E., SCHEPER, G. C., ABBINK, T. E., HEINE, V. M. & VAN DER KNAAP, M. S. 2016. Astrocytes are central in the pathomechanisms of vanishing white matter. *J Clin Invest,* 126**,** 1512-24.

DZHAGALOV, I., ST JOHN, A. & HE, Y. W. 2007. The antiapoptotic protein Mcl-1 is essential for the survival of neutrophils but not macrophages. *Blood,* 109**,** 1620-6.

760 EDDLESTON, M. & MUCKE, L. 1993. Molecular profile of reactive astrocytes--implications for
761 their role in neurologic disease. *Neuroscience,* 54**,** 15-36.
762 ELROY-STEIN, O. 2017. Mitochondrial malfunction in vanishing white matter disease: a
763 disease of the cytosolic translation machinery. *Neural Regen Res,* 12**,** 1610-1612.
764 FOGARTY, L. C., FLEMMER, R. T., GEIZER, B. A., LICURSI, M., KARUNANITHY, A., OPFERMAN,
765 J. T., HIRASAWA, K. & VANDERLUIT, J. L. 2019. Mcl-1 and Bcl-xL are essential for
766 survival of the developing nervous system. *Cell Death Differ,* 26**,** 1501-1515.
767 FOGLI, A., WONG, K., EYMARD-PIERRE, E., WENGER, J., BOUFFARD, J. P., GOLDIN, E., BLACK,
768 D. N., BOESPFLUG-TANGUY, O. & SCHIFFMANN, R. 2002. Cree leukoencephalopathy
769 and CACH/VWM disease are allelic at the EIF2B5 locus. *Ann Neurol,* 52**,** 506-10.
770 FRITSCH, R. M., SCHNEIDER, G., SAUR, D., SCHEIBEL, M. & SCHMID, R. M. 2007. Translational
771 repression of MCL-1 couples stress-induced eIF2 alpha phosphorylation to
772 mitochondrial apoptosis initiation. *J Biol Chem,* 282**,** 22551-62.
773 GEVA, M., CABILLY, Y., ASSAF, Y., MINDROUL, N., MAROM, L., RAINI, G., PINCHASI, D. &
774 ELROY-STEIN, O. 2010. A mouse model for eukaryotic translation initiation factor 2B-
775 leucodystrophy reveals abnormal development of brain white matter. *Brain,* 133**,**
776 2448-61.
777 GLASGOW, S. M., ZHU, W., STOLT, C. C., HUANG, T. W., CHEN, F., LOTURCO, J. J., NEUL, J. L.,
778 WEGNER, M., MOHILA, C. & DENEEN, B. 2014. Mutual antagonism between Sox10
779 and NFIA regulates diversification of glial lineages and glioma subtypes. *Nat*
780 *Neurosci,* 17**,** 1322-9.
781 GUYENET, S. J., FURRER, S. A., DAMIAN, V. M., BAUGHAN, T. D., LA SPADA, A. R. & GARDEN,
782 G. A. 2010. A simple composite phenotype scoring system for evaluating mouse
783 models of cerebellar ataxia. *J Vis Exp*.
784 HASAN, S. M., SHEEN, A. D., POWER, A. M., LANGEVIN, L. M., XIONG, J., FURLONG, M., DAY,
785 K., SCHUURMANS, C., OPFERMAN, J. T. & VANDERLUIT, J. L. 2013. Mcl1 regulates the
786 terminal mitosis of neural precursor cells in the mammalian brain through p27Kip1.
787 *Development,* 140**,** 3118-27.
788 HATTEN, M. E. 1990. Riding the glial monorail: a common mechanism for glial-guided
789 neuronal migration in different regions of the developing mammalian brain. *Trends*
790 *Neurosci,* 13**,** 179-84.
791 HERRERO, M., MANDELBOUM, S. & ELROY-STEIN, O. 2019. eIF2B Mutations Cause
792 Mitochondrial Malfunction in Oligodendrocytes. *Neuromolecular Med,* 21**,** 303-313.
793 IMAI, Y., IBATA, I., ITO, D., OHSAWA, K. & KOHSAKA, S. 1996. A novel gene iba1 in the major
794 histocompatibility complex class III region encoding an EF hand protein expressed in
795 a monocytic lineage. *Biochem Biophys Res Commun,* 224**,** 855-62.
796 ITO, D., IMAI, Y., OHSAWA, K., NAKAJIMA, K., FUKUUCHI, Y. & KOHSAKA, S. 1998. Microglia-
797 specific localisation of a novel calcium binding protein, Iba1. *Brain Res Mol Brain Res,*
798 57**,** 1-9.
799 KANTOR, L., HARDING, H. P., RON, D., SCHIFFMANN, R., KANESKI, C. R., KIMBALL, S. R. &
800 ELROY-STEIN, O. 2005. Heightened stress response in primary fibroblasts expressing
801 mutant eIF2B genes from CACH/VWM leukodystrophy patients. *Hum Genet,* 118**,** 99-
802 106.
803 KOHLER, W., CURIEL, J. & VANDERVER, A. 2018. Adulthood leukodystrophies. *Nat Rev*
804 *Neurol,* 14**,** 94-105.
805 KOHLSCHUTTER, A. & EICHLER, F. 2011. Childhood leukodystrophies: a clinical perspective.
806 *Expert Rev Neurother,* 11**,** 1485-96.

807 KUANG, Y., LIU, Q., SHU, X., ZHANG, C., HUANG, N., LI, J., JIANG, M. & LI, H. 2012. Dicer1 and
808 MiR-9 are required for proper Notch1 signaling and the Bergmann glial phenotype in
809 the developing mouse cerebellum. *Glia,* 60**,** 1734-46.
810 LANG, P. Y., NANJANGUD, G. J., SOKOLSKY-PAPKOV, M., SHAW, C., HWANG, D., PARKER, J.
811 S., KABANOV, A. V. & GERSHON, T. R. 2016. ATR maintains chromosomal integrity
812 during postnatal cerebellar neurogenesis and is required for medulloblastoma
813 formation. *Development,* 143**,** 4038-4052.
814 LEEGWATER, P. A., VERMEULEN, G., KONST, A. A., NAIDU, S., MULDERS, J., VISSER, A.,
815 KERSBERGEN, P., MOBACH, D., FONDS, D., VAN BERKEL, C. G., LEMMERS, R. J.,
816 FRANTS, R. R., OUDEJANS, C. B., SCHUTGENS, R. B., PRONK, J. C. & VAN DER KNAAP,
817 M. S. 2001. Subunits of the translation initiation factor eIF2B are mutant in
818 leukoencephalopathy with vanishing white matter. *Nat Genet,* 29**,** 383-8.
819 MALONE, C. D., HASAN, S. M., ROOME, R. B., XIONG, J., FURLONG, M., OPFERMAN, J. T. &
820 VANDERLUIT, J. L. 2012. Mcl-1 regulates the survival of adult neural precursor cells.
821 *Mol Cell Neurosci,* 49**,** 439-47.
822 MELCHIONDA, L., HAACK, T. B., HARDY, S., ABBINK, T. E., FERNANDEZ-VIZARRA, E.,
823 LAMANTEA, E., MARCHET, S., MORANDI, L., MOGGIO, M., CARROZZO, R., TORRACO,
824 A., DIODATO, D., STROM, T. M., MEITINGER, T., TEKTURK, P., YAPICI, Z., AL-
825 MURSHEDI, F., STEVENS, R., RODENBURG, R. J., LAMPERTI, C., ARDISSONE, A.,
826 MORONI, I., UZIEL, G., PROKISCH, H., TAYLOR, R. W., BERTINI, E., VAN DER KNAAP,
827 M. S., GHEZZI, D. & ZEVIANI, M. 2014. Mutations in APOPT1, encoding a
828 mitochondrial protein, cause cavitating leukoencephalopathy with cytochrome c
829 oxidase deficiency. *Am J Hum Genet,* 95**,** 315-25.
830 NAKAMURA, A., SWAHARI, V., PLESTANT, C., SMITH, I., MCCOY, E., SMITH, S., MOY, S. S.,
831 ANTON, E. S. & DESHMUKH, M. 2016. Bcl-xL Is Essential for the Survival and Function
832 of Differentiated Neurons in the Cortex That Control Complex Behaviors. *J Neurosci,*
833 36**,** 5448-61.
834 NISHIYAMA, A., BOSHANS, L., GONCALVES, C. M., WEGRZYN, J. & PATEL, K. D. 2016. Lineage,
835 fate, and fate potential of NG2-glia. *Brain Res,* 1638**,** 116-128.
836 OCASIO, J. K., BATES, R. D. P., RAPP, C. D. & GERSHON, T. R. 2019. GSK-3 modulates SHH-
837 driven proliferation in postnatal cerebellar neurogenesis and medulloblastoma.
838 *Development,* 146.
839 RAINI, G., SHARET, R., HERRERO, M., ATZMON, A., SHENOY, A., GEIGER, T. & ELROY-STEIN,
840 O. 2017. Mutant eIF2B leads to impaired mitochondrial oxidative phosphorylation in
841 vanishing white matter disease. *J Neurochem,* 141**,** 694-707.
842 RAKIC, P. 1971. Neuron-glia relationship during granule cell migration in developing
843 cerebellar cortex. A Golgi and electronmicroscopic study in Macacus Rhesus. *J Comp*
844 *Neurol,* 141**,** 283-312.
845 RAYMOND, G. V. 2017. Leukodystrophy: Basic and Clinical. *Adv Neurobiol,* 15**,** 365-382.
846 SAHIN KAYA, S., MAHMOOD, A., LI, Y., YAVUZ, E. & CHOPP, M. 1999. Expression of nestin
847 after traumatic brain injury in rat brain. *Brain Res,* 840**,** 153-7.
848 SCHMIDT-KASTNER, R., AGUIRRE-CHEN, C., SAUL, I., YICK, L., HAMASAKI, D., BUSTO, R. &
849 GINSBERG, M. D. 2005. Astrocytes react to oligemia in the forebrain induced by
850 chronic bilateral common carotid artery occlusion in rats. *Brain Res,* 1052**,** 28-39.
851 TAMAGNO, I. & SCHIFFER, D. 2006. Nestin expression in reactive astrocytes of human
852 pathology. *J Neurooncol,* 80**,** 227-33.

TECH, K., TIKUNOV, A. P., FAROOQ, H., MORRISSY, A. S., MEIDINGER, J., FISH, T., GREEN, S. C., LIU, H., LI, Y., MUNGALL, A. J., MOORE, R. A., MA, Y., JONES, S. J. M., MARRA, M. A., VANDER HEIDEN, M. G., TAYLOR, M. D., MACDONALD, J. M. & GERSHON, T. R. 2017. Pyruvate Kinase Inhibits Proliferation during Postnatal Cerebellar Neurogenesis and Suppresses Medulloblastoma Formation. *Cancer Res,* 77**,** 3217-3230.

VAN DER KNAAP, M. S., BARTH, P. G., GABREELS, F. J., FRANZONI, E., BEGEER, J. H., STROINK, H., ROTTEVEEL, J. J. & VALK, J. 1997. A new leukoencephalopathy with vanishing white matter. *Neurology,* 48**,** 845-55.

VAN DER KNAAP, M. S. & BUGIANI, M. 2017. Leukodystrophies: a proposed classification system based on pathological changes and pathogenetic mechanisms. *Acta Neuropathol,* 134**,** 351-382.

VAN DER KNAAP, M. S. & BUGIANI, M. 2018. Leukodystrophies - much more than just diseases of myelin. *Nat Rev Neurol,* 14**,** 747-748.

VAN DER KNAAP, M. S., FOGLI, A., BOESPFLUG-TANGUY, O., ABBINK, T. E. M. & SCHIFFMANN, R. 1993. Childhood Ataxia with Central Nervous System Hypomyelination / Vanishing White Matter. *In:* ADAM, M. P., ARDINGER, H. H., PAGON, R. A., WALLACE, S. E., BEAN, L. J. H., STEPHENS, K. & AMEMIYA, A. (eds.) *GeneReviews((R)).* Seattle (WA).

VAN DER KNAAP, M. S., PRONK, J. C. & SCHEPER, G. C. 2006. Vanishing white matter disease. *Lancet Neurol,* 5**,** 413-23.

VANDERVER, A., TONDUTI, D., SCHIFFMANN, R., SCHMIDT, J. & VAN DER KNAAP, M. S. 1993. Leukodystrophy Overview - ARCHIVED CHAPTER, FOR HISTORICAL REFERENCE ONLY. *In:* ADAM, M. P., ARDINGER, H. H., PAGON, R. A., WALLACE, S. E., BEAN, L. J. H., STEPHENS, K. & AMEMIYA, A. (eds.) *GeneReviews((R)).* Seattle (WA).

YASUDA, O., FUKUO, K., SUN, X., NISHITANI, M., YOTSUI, T., HIGUCHI, M., SUZUKI, T., RAKUGI, H., SMITHIES, O., MAEDA, N. & OGIHARA, T. 2006. Apop-1, a novel protein inducing cyclophilin D-dependent but Bax/Bak-related channel-independent apoptosis. *J Biol Chem,* 281**,** 23899-907.

ZHOU, L., LI, P., CHEN, N., DAI, L. F., GAO, K., LIU, Y. N., SHEN, L., WANG, J. M., JIANG, Y. W. & WU, Y. 2019. Modeling vanishing white matter disease with patient-derived induced pluripotent stem cells reveals astrocytic dysfunction. *CNS Neurosci Ther,* 25**,** 759-771.

ZHUO, L., THEIS, M., ALVAREZ-MAYA, I., BRENNER, M., WILLECKE, K. & MESSING, A. 2001. hGFAP-cre transgenic mice for manipulation of glial and neuronal function in vivo. *genesis,* 31**,** 85-94.